Figure 4. Neuronal activities during SWs are optically imaged. A. A confocal image of the CA1 stratum pyramidale in an OGB1-loaded slice. The location of an LFP electrode is shown by the white lines. **B.** Example of calcium transients from 9 cells and LFP trace, before (left) and after (right) SKF38393 application. **C.** Simultaneous cell-attached recording and calcium imaging. Numbers of spikes are represented above each spike. Spike timimgs detected from the calcium trace are shown by bars below the trace. **D.** A peri-SW time histogram of calcium events. Data are the means ± SEMs from 8 slices, including a total of 7,709 calcium events emitted by 199 cells. The time period between −200 ms and 50 ms relative to the SW peak was defined as a SW window (shadow). Calcium events during this time window are regarded as SW-locked activities. **E.** Representative raster plots of calcium events 0–3 min before (top) and 15–18 min after (bottom) the bath application of 30 μM SKF38393. Green or orange bars above each raster plot indicate the time stamps of individual SW events. Thick dots in the rastergram indicate SW-locked activities. **F–H.** Comparisons of peri-SW time histograms from each slices in 3 parameters; Time lag of the histogram peak from the SW peak (F), skewness of the histograms (G) and kurtosis of the histograms (H). **I.** Comparisons of the co-activation probability of any given pairs of cells that participated at least once in SW before (left) and after (right) the drug application. Each dot indicates a single neuron pair.
doi:10.1371/journal.pone.0104438.g004

relationship between the number of SW-participating neurons and the number of patterns. These two values were not correlated (Fig. 7G, Before (green); $R^2 = 0.21$, $P = 0.24$. After (orange); $R^2 = 8.3 \times 10^{-4}$, $P = 0.95$). Thus, the effect of the increased chance of possible cell combinations on the increased SW patterns was, if any, minimal.

Finally, we sought to confirm this conclusion at a different level of neuronal activity. The SW patterns are reported to be reflected in SW-related LFP spectrum patterns [30,31,43,44]. Indeed, we found diverse SW patterns in the LFP spectra (Fig. 8A). We thus applied the same clustering method to the correlation coefficients between the LFP spectrum patterns (Fig. 8B). The number of SW clusters increased after SKF38393 treatment (Fig. 8C right; $P = 0.0059$, $t_7 = 3.38$, paired t-test, $n = 8$ slices), while this tendency is not observed in the control group (Fig. 8C left; $P = 0.69$, $t_4 = 0.53$, paired t-test, $n = 5$ slices).

Discussion

We demonstrated that a brief bath-application of dopamine to hippocampal slices induced a long-lasting increase in the SW event frequency through dopamine D_1/D_5 receptor activation. The D_1/D_5 receptor activation did not largely change SW-participating neurons and the number of neurons involved in single SWs, but it reorganized combinations of neurons co-participating in SWs and thereby expanded the diversity of the internal structures of SWs. D_1/D_5 receptor activation is reported to suppress cholinergically induced gamma oscillations [45]. On the other hand, a decreased level of cholinergic tone is associated with the SW/ripple-rich state of hippocampal networks [46], and we have previously demonstrated that cholinergic receptor activation suppresses the occurrence of SW/ripples [23]. Recent studies have demonstrated that SW/ripple-related firing increases in frequency in slices that received cholinergic stimulation, and such specific enrichment of SW/ripples may be linked to the efficiency of memory consolidation [47,48]. Therefore, dopamine-induced increases in SW repertoires may be associated with an enrichment of episodic-like contexts encoded in memories.

CA3 neurons that fire in ripple events are known to increase in number when rats are rewarded [9]. In our study, dopamine receptor activation did not significantly change the power of CA1 ripple oscillations or the number of CA1 neurons that were activated in single SW events, but it readily increased the amplitude of SWs. SWs are recorded as sharp sources of the field potentials in CA1 stratum pyramidale and are likely to reflect synaptic inputs from CA3 neurons [34] (although caution must be taken to interpret what the SW components mean, especially when LFPs were recorded from the soma; because they do not directly measure the pure sum of synaptic activity (or spiking activity) of individual excitatory neurons and are often contaminated with active sources of somatic inhibition). This idea that dopamine-induced increase in the SW size suggests an increased level of synaptic inputs is consistent with the fact that after reward stimulation, ripple events come to recruit more CA3 neurons [9]. fMCI from the CA3 region is required to confirm this hypothesis, but unfortunately, it is extremely difficult to load CA3 neurons with calcium indicators, due to unknown reasons (unpublished data).

An apparent contradiction is that neither the ripple power nor the number of calcium events in a SW event accompanied the increased SW amplitude, suggesting that stronger synaptic inputs did not lead to more spike outputs. During SW/ripples, pyramidal cells as well as inhibitory interneurons, such as basket cells and bistratified cells, increase their firing rates [35]. We have recently shown that the SW amplitude correlates with the strength of SW-relevant phasic inhibitory inputs as well as excitatory inputs [40]. Therefore, synaptic inputs to CA1 pyramidal cells are likely balanced between excitation and inhibition during SWs [24,49,50] and thereby may provide the homeostatic properties of CA1 network excitability, as opposed to increased CA3 excitation during SW/ripples.

We directly evaluated the pattern change in individual SWs by utilizing the affinity propagation algorithm. This algorithm allowed us to detect the latent cliqueness underlying SWs based on their internal patterns. Interestingly, although dopamine receptor activation did not change the overall tendency of individual neurons to participate in SWs or the mean number of neurons involved in a single SW, it readily reorganized subsets of neurons that participated jointly in SWs. As a result, dopamine increased the total number of SW categories. However, possible is another trivial explanation that the increased repertoires was merely a mathematical consequence of an increase in the total number of active neurons. In other words, the effect may be due partly to more visibility of the latent network through an emergence of previously silent interactions. Although the slight increase in SW-participated neurons after SKF38393 administration was not statistically significant, our results cannot alone determine whether higher activation of individual neurons led to an apparent increase in neuronal ensemble repertoires or whether the network actively recruited a more number of neuronal interactions in order to increase the repertoires.

We imaged calcium activities at 50 Hz and cannot dissolve sequential activation of SW-participating neurons [51–54]. It will be interesting to see dopamine-induced changes in spike sequence patterns. To this end, faster image acquisition is needed. Moreover, fMCI using chemical dyes does not allow us to distinguish pyramidal neurons from GABAergic interneurons. Our data would be more informative if the activity patterns can be dissociated between different types of neurons. Using a targeted patch-clamp recording technique, we have recently demonstrated that interneurons fire action potentials during almost all SW events [40]. Because their firing patterns are rather homogenous compared to a rich repertoire of pyramidal neuron activity.

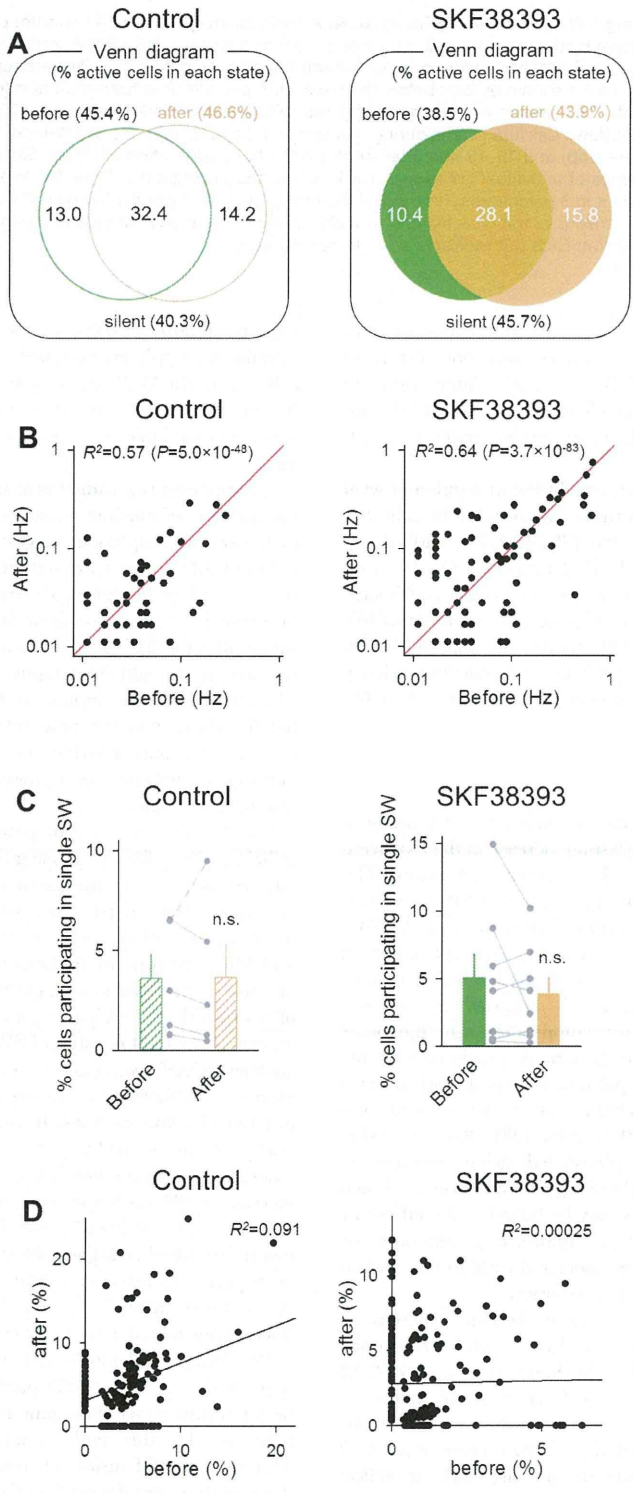

Figure 5. SKF38393 preserves SWs-participating neurons. A. A Venn diagram of the population of cells that participated in at least one SW event during the 3-min periods before and after the application of control aCSF (left) or 30 μM SKF38393 (right). The values indicate the percentage of cells involved in the corresponding states to the total cells. The two populations overlapped significantly. Control: $P = 1.85 \times 10^{-5}$ *versus* the chance level (21.2%), $Z = 4.28$; SKF38393: $P = 1.62 \times 10^{-8}$ versus the chance level (16.9%), $Z = 5.65$, Z-test for a proportion. **B.** Relationship of the frequencies of SW-locked activities of individual neurons before and after control aCSF (left) or 30 μM SKF38393 (right) administration. Each dot indicates a single neuron. Control: $R^2 = 0.57$, $P = 5.0 \times 10^{-48}$, $t_{251} = 18.3$; SKF38393: $R^2 = 0.64$, $P = 3.7 \times 10^{-83}$, $t_{364} = 25.5$, *t*-test of a correlation coefficient. **C.** The mean

percentage of cells that participated in a single SW event to the total cells before and after aCSF or SKF38393 administration. Each gray dataset represents a single slice. Control: $P=0.93$, $t_4=0.098$; SKF38393: $P=0.25$, $t_7=1.23$, paired t-test. Data are the means ± SEMs of 5 or 8 slices. **D.** Comparison of the mean amplitudes of SW-locked calcium transients from 150 and 199 SW participants before and after the drug application. Control: $R^2=0.091$, SKF38393, $R^2=0.00025$, $P=0.13$, $Z=1.53$, Z-test for two correlation coefficients. Each dot indicates a single neuron.
doi:10.1371/journal.pone.0104438.g005

Therefore, we believe that interneurons are unlikely to finely modulate (or be modulated by) the SW activity patterns.

Under *in vivo* conditions, sets of place cells that were activated prior to reward stimuli are preferentially reactivated in subsequent SW/ripples. Our *in vitro* work failed to show that the increased repertories of SWs arose from increased occurrence of a specific set of "rewarded" SWs that had rarely emerged during the baseline period. To assess whether dopamine facilitates SWs in a pattern-specific manner, investigations using online closed loop-driven, SW pattern-triggered activation of dopamine receptors is necessary. Recently available dopamine-related optogenetic tools [55] or caged-dopamine reagents [56] will help this approach.

In conclusion, this study provides an insight into the cellular mechanisms for reward-enhanced memory consolidation in terms of SW/ripples. It is also intriguing to interpret our data in relation to the dopamine hypothesis of schizophrenia. Dopamine release is increased in patients with schizophrenia [57], and an experimental mouse model of schizophrenia exhibits an aberrantly increased level of SW/ripples [54]. Combining a pattern-specific closed-loop system with behavioral assessments will reveal a causal link

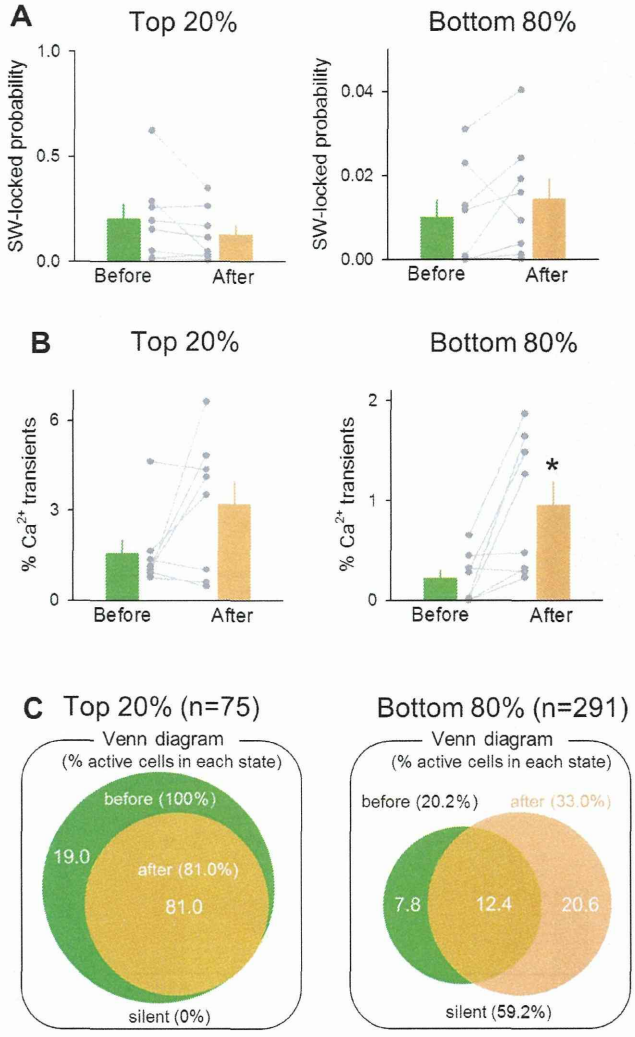

Figure 6. Putative pyramidal neurons are more affected by SKF38393 than putative interneurons. A. The mean SW-locked probability of cells with the top 20% SW-locked probability (left) and that of the bottom 80% SW-locked probability (right). **B.** The mean amplitude of calcium transients of the top 20% SW-locking cells (left) and that of the bottom 80% cells (right; $^*P=0.016$, $t_7=3.14$, paired t-test). **C.** A Venn diagram of the population of cells that participated in at least one SW event during the 3-min periods before and after the application 30 μM SKF38393 for the top 20% SW-locking cells (left) and the bottom 80% cells (right).
doi:10.1371/journal.pone.0104438.g006

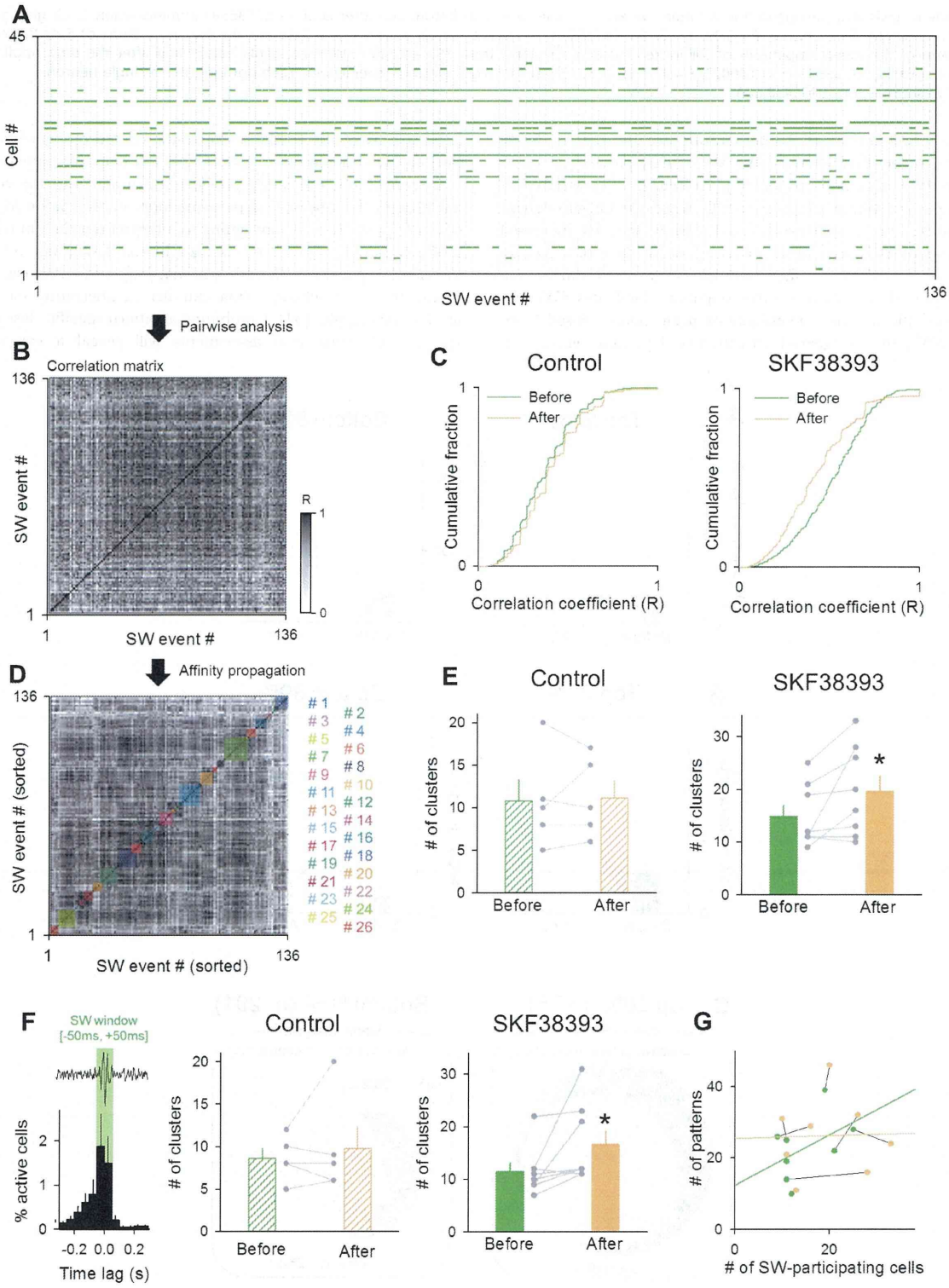

Figure 7. SKF38393 increases the repertoires of SW-relevant firing patterns. A. Representative spatiotemporal patterns of SW-locked activities in 136 SW events during the observation period of 3 min. **B.** The correlation coefficients between patterns of SW-participating neurons were calculated for all possible SW pairs. The representative correlation matrix was obtained from 136 SWs shown in A. **C.** Cumulative distribution of the correlation coefficients before (green) and after (orange) perfusion with control aCSF [left, 795 SW events (before) and 1,076 (after) from 8 slices] and SKF38393 [right, 795 SW events (before) and 1,076 (after) from 8 slices]. **D.** The affinity propagation algorithm separated 136 SW events in B. into 26

SW subgroups, indicated by different colors. **E.** The mean number of the SW subgroups before and after the application of control aCSF (left) and SKF38393 (right). Each gray dataset indicates a single slice. *$P = 0.030$, $t_7 = 2.25$, paired *t*-test. Data are the means ± SEMs of 5 or 8 slices. **F.** The same analysis as E was repeated a time window between −50 and +50 ms relative to the SW peak (left). The mean numbers of the SW subgroups before and after the application of control aCSF (left) and SKF38393 (right) are shown in the bar graph. *$P = 0.036$, $t_7 = 2.12$, paired *t*-test. Data are the means ± SEMs of 8 slices. **G.** The relationship between the number of SW-participating neurons and of SW patterns. Data obtained from the same slice are connected with black line. Before (green); $R^2 = 0.21$, $P = 0.24$. After (orange); $R^2 = 8.3 \times 10^{-4}$, $P = 0.95$.
doi:10.1371/journal.pone.0104438.g007

between dopaminergic SW modulation and its behavioral consequence.

Methods

Animal ethics

Experiments were performed with the approval of the animal experiment ethics committee at the University of Tokyo (approval number: P24-8) and according to the University of Tokyo guidelines for the care and use of laboratory animals.

Drug

Dopamine dihydrochloride (Sigma-Aldrich, St Louis, MO), SCH23390 (Tocris-Bioscience, Bristol, UK), (S)-(−)-sulpiride (Sigma-Aldrich), and SKF38393 hydrochloride (Sigma-Aldrich) were dissolved at 10 mM in water and stocked at 4°C. Immediately before use, they were diluted to the final concentration with aCSF containing (in mM): 127 NaCl (Nacalai Tesque, Kyoto, Japan), 1.6 KCl (Wako, Tokyo, Japan), 1.24 KH_2PO_4 (Nacalai Tesque), 1.3 $MgSO_4$ (Nacalai Tesque), 2.4 $CaCl_2$ (Wako), 26 $NaHCO_3$ (Wako), and 10 D-glucose (Wako).

Slice Preparation

Acute slices were prepared from the hippocampal formation of male 3-to-4-week-old ICR mice. Mice were anesthetized with ether and decapitated, and a posterior brain block (400 μm thick) was obliquely cut at an angle of 12.7° in the fronto-occipital direction using a vibratome in ice-cold oxygenated cutting solution consisting of (in mM) 222.1 sucrose, 27 $NaHCO_3$, 1.4 NaH_2PO_4, 2.5 KCl, 1 $CaCl_2$, 7 $MgSO_4$, 0.5 ascorbic acid [23,58]. Slices were transferred to an interface chamber containing oxygenated aCSF at 35°C and were allowed to recover for at least 1.5 h. On average, 2–4 slices were obtained from one brain.

Electrophysiological recording

Experiments were performed in a submerged chamber perfused at 7–9 ml/min with oxygenated aCSF at 35–37°C. LFPs were recorded from CA1 stratum pyramidale using borosilicate glass pipettes (1–2 MΩ) filled with aCSF. Signals were amplified by MultiClamp 700B (Molecular Devices, Union City, CA, USA), digitized at 10,000 Hz and filtered with a band of 1–2,000 Hz by pCLAMP 10 (Molecular Devices). Offline analysis was conducted using custom-made MATLAB routines (MathWorks, Natick, MA,

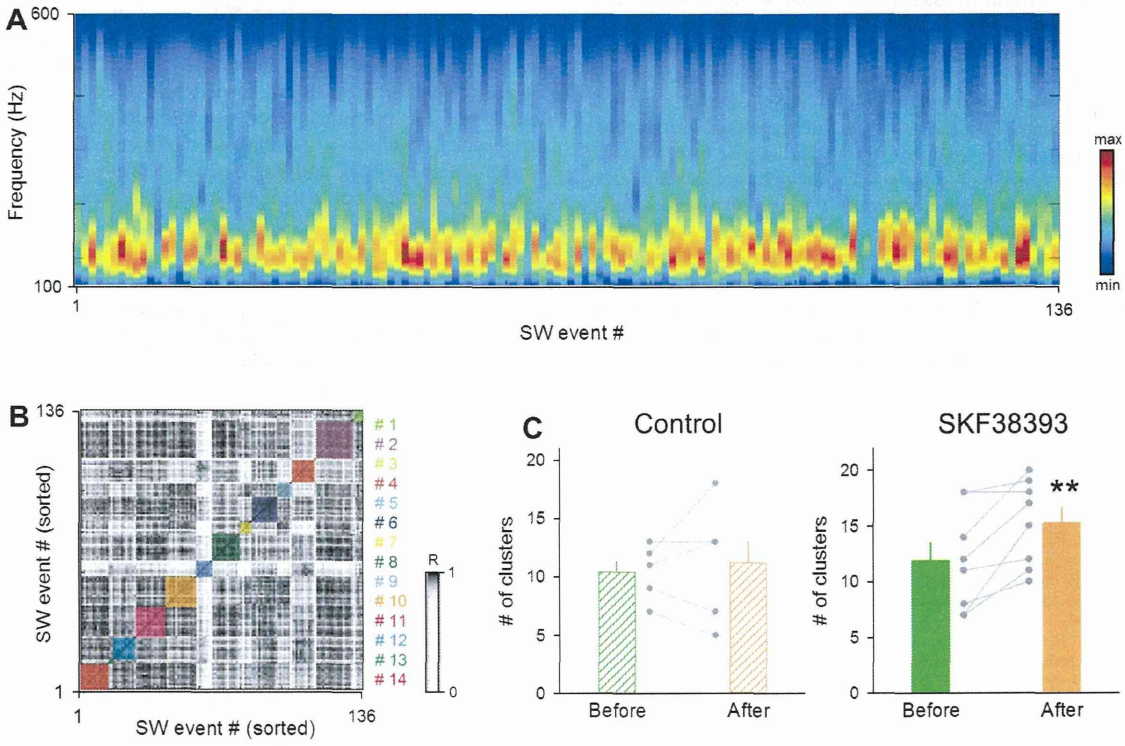

Figure 8. SKF38393 increases the repertoires of SW-relevant LFP spectra patterns. A. Representative fast Fourier transform spectra of 136 SW events during the pre-treatment baseline period of 3 min. **B.** The correlation matrix obtained from the 136 SWs was sorted by the affinity propagation and was clustered into 14 SW subgroups. **C.** The mean numbers of the SW subgroups before and after administration with control aCSF (left) and SKF38393 (right). Each gray dataset indicates a single slice. **$P = 0.0059$, $t_7 = 3.38$, paired *t*-test. Data are the means ± SEMs of 8 slices.
doi:10.1371/journal.pone.0104438.g008

USA). To detect SW/ripples, LFP traces were band-pass filtered at 2–30 Hz and were thresholded at 4 times above the SD of the baseline noise. The detected SW events were scrutinized by eye and manually rejected if they were erroneously detected. Cell-attached patch-clamp recordings were obtained from CA1 pyramidal neurons with an Axopatch 700B amplifier (Molecular Devices). Borosilicate glass pipettes (4–7 MΩ) were filled with aCSF. Signals were low-pass filtered at 1–2 kHz, digitized at 20 kHz and analysed with pCLAMP 10.2 software (Molecular Devices). fEPSPs were recorded at room temperature. Stimuli were delivered through bipolar tungsten electrodes placed in the CA1 stratum radiatum to stimulate Schaffer collaterals, and fEPSPs were recorded from the CA1 stratum radiatum using glass pipettes filled with aCSF. Test pulses with a duration of 100 μs was given every 30 s, and the stimulus intensity was set at about 30% of the maximum amplitude of fEPSPs. Changes in fEPSPs were expressed as a percentage change in their amplitudes and maximal slopes, relative to the mean values during the baseline period of −15 to 0 min).

Optical recording

fMCI was conducted using acute slices loaded locally with OGB1-AM [36]. Fluorophores were excited at 488 nm and visualized using a 507-nm long-pass emission filter. Videos were at 50 frames/s using a 16× objective (CFI75LWD16xW, Nikon, Tokyo, Japan), a Nipkow-disk confocal microscope (CSU-X1; Yokogawa Electric, Tokyo, Japan), and a cooled EM-CCD camera (iXon DU897, Andor, Belfast, UK). The fluorescence change was measured as $(F_t-F_0)/F_0$, where the F_t is the fluorescence intensity at a given time point; F_0 is the baseline. Spike-elicited calcium transients were automatically detected and visually inspected [59]. Our automatic algorithm was composed of two steps, *i.e.*, a conditioning (learning) phase and a test (spike detection) phase. In the conditioning phase, the parameters were tuned to give the most appropriate probability of spike detection from sample datasets. In the test phase, the algorithm with the best tuned parameters was used to extract spike signals from datasets different from those used in the conditioning phase. The data used for conditioning was collected from 10 cells. All routines were written in MATLAB (Math Works). Co-activation probability within a SW was calculated for any pair of cells that participated at least once in SWs. The probability for cell A and cell B was given as $N(A\cap B)/(N(A)+N(B)-N(A\cap B))$, where $N(A\cap B)$ is the number of SWs in which cell A and cell B fired in the same SW events, and $N(A)$ (or $N(B)$) is the number of SWs in which cell A (or cell B) participated. The co-activation probability without SWs was calculated for any pair of cells that fired at least once during the period without SWs *i.e.* activities that occurred outside the SW period *i.e.*, from −200 ms to +50 ms relative to the SW peak. Two spikes that occurred within 250 ms was defined as co-activated firing. The co-activation probability for cell A and cell B was $N(A\cap B)/(N(A)+N(B)-N(A\cap B))$, where $N(A\cap B)$ is the total number of co-activated events, and $N(A)$ (or $N(B)$) was the total number of spikes of cell A (or B) during SW-free periods. A time bin of 20 ms was used to evaluate the shapes of the distribution of calcium transients that occurred within 500 ms relative to the SW peak. For each neuron, the total number of calcium transients within SW periods was divided by the recording period (3 min) and was defined as the SW-locked activity frequency of the neurons.

Statistical Analysis

The affinity propagation was performed with custom-written MATLAB software [41]. The correlation matrix, which represents the similarity between all possible SW pairs, was calculated from a Cell-SW matrix and was treated with the algorithm. The clustering was conducted by iteratively passing "messages" between the data points until it reached the equilibrium. Specifically, for the first step, the "responsibility" was passed from a point to any other points. The responsibility means how comparatively suitable a point is to be the exemplar for another point rather than any other point. For the second step, the "availability" was passed from a point to any other points. The availability means how comparatively appropriate it would be for any other points to pick message-sending point as its exemplar. The affinity propagation for LFP traces was performed in the same way, but now using a spectrum-SW matrix in which each row corresponded with the ripple power in fast Fourier transform at a band filter of 100–600 Hz. The bin used was 1 Hz. We reported data as the means ± SEMs unless specified otherwise. Student's *t*-test, *Z*-test for the equality of two proportions, *Z*-test for a proportion, *t*-test for a correlation coefficient, *Z*-test for two correlation coefficients, and Kolmogorov-Smirnov test were used to assess the significance of the differences. $P<0.05$ was considered statistically significant.

Author Contributions

Conceived and designed the experiments: TM HN YI. Performed the experiments: TM HN TI YW. Analyzed the data: TM HN. Contributed reagents/materials/analysis tools: TM NM YI. Wrote the paper: TM YI.

References

1. Buzsaki G (1986) Hippocampal sharp waves: their origin and significance. Brain Res 398: 242–252.
2. Ylinen A, Bragin A, Nadasdy Z, Jando G, Szabo I, et al. (1995) Sharp wave-associated high-frequency oscillation (200 Hz) in the intact hippocampus: network and intracellular mechanisms. J Neurosci 15: 30–46.
3. Chrobak JJ, Buzsaki G (1996) High-frequency oscillations in the output networks of the hippocampal-entorhinal axis of the freely behaving rat. J Neurosci 16: 3056–3066.
4. Norimoto H, Matsumoto N, Miyawaki T, Matsuki N, Ikegaya Y (2013) Subicular activation preceding hippocampal ripples in vitro. Sci Rep 3: 2696.
5. Buzsaki G (1989) Two-stage model of memory trace formation: a role for "noisy" brain states. Neuroscience 31: 551–570.
6. Lee AK, Wilson MA (2002) Memory of sequential experience in the hippocampus during slow wave sleep. Neuron 36: 1183–1194.
7. Girardeau G, Benchenane K, Wiener SI, Buzsaki G, Zugaro MB (2009) Selective suppression of hippocampal ripples impairs spatial memory. Nat Neurosci 12: 1222–1223.
8. Cheng S, Frank LM (2008) New experiences enhance coordinated neural activity in the hippocampus. Neuron 57: 303–313.
9. Singer AC, Frank LM (2009) Rewarded outcomes enhance reactivation of experience in the hippocampus. Neuron 64: 910–921.
10. Schultz W (1998) Predictive reward signal of dopamine neurons. J Neurophysiol 80: 1–27.
11. Horvitz JC (2000) Mesolimbocortical and nigrostriatal dopamine responses to salient non-reward events. Neuroscience 96: 651–656.
12. Akil H, Watson SJ, Young E, Lewis ME, Khachaturian H, et al. (1984) Endogenous opioids: biology and function. Annu Rev Neurosci 7: 223–255.
13. Di Sebastiano AR, Coolen LM (2012) Orexin and natural reward: feeding, maternal, and male sexual behavior. Prog Brain Res 198: 65–77.
14. Hyman SE, Malenka RC, Nestler EJ (2006) Neural mechanisms of addiction: the role of reward-related learning and memory. Annu Rev Neurosci 29: 565–598.
15. Gasbarri A, Sulli A, Packard MG (1997) The dopaminergic mesencephalic projections to the hippocampal formation in the rat. Prog Neuropsychopharmacol Biol Psychiatry 21: 1–22.
16. Ihalainen JA, Riekkinen P, Jr., Feenstra MG (1999) Comparison of dopamine and noradrenaline release in mouse prefrontal cortex, striatum and hippocampus using microdialysis. Neurosci Lett 277: 71–74.

17. Bernabeu R, Bevilaqua L, Ardenghi P, Bromberg E, Schmitz P, et al. (1997) Involvement of hippocampal cAMP/cAMP-dependent protein kinase signaling pathways in a late memory consolidation phase of aversively motivated learning in rats. Proc Natl Acad Sci U S A 94: 7041–7046.
18. Bethus I, Tse D, Morris RG (2010) Dopamine and memory: modulation of the persistence of memory for novel hippocampal NMDA receptor-dependent paired associates. J Neurosci 30: 1610–1618.
19. Kubota D, Colgin LL, Casale M, Brucher FA, Lynch G (2003) Endogenous waves in hippocampal slices. J Neurophysiol 89: 81–89.
20. Maier N, Nimmrich V, Draguhn A (2003) Cellular and network mechanisms underlying spontaneous sharp wave-ripple complexes in mouse hippocampal slices. J Physiol 550: 873–887.
21. Behrens CJ, van den Boom LP, de Hoz L, Friedman A, Heinemann U (2005) Induction of sharp wave-ripple complexes in vitro and reorganization of hippocampal networks. Nat Neurosci 8: 1560–1567.
22. Wu C, Asl MN, Gillis J, Skinner FK, Zhang L (2005) An in vitro model of hippocampal sharp waves: regional initiation and intracellular correlates. J Neurophysiol 94: 741–753.
23. Norimoto H, Mizunuma M, Ishikawa D, Matsuki N, Ikegaya Y (2012) Muscarinic receptor activation disrupts hippocampal sharp wave-ripples. Brain Res 1461: 1–9.
24. Hajos N, Karlocai MR, Nemeth B, Ulbert I, Monyer H, et al. (2013) Input-output features of anatomically identified CA3 neurons during hippocampal sharp wave/ripple oscillation in vitro. J Neurosci 33: 11677–11691.
25. Hajos N, Ellender TJ, Zemankovics R, Mann EO, Exley R, et al. (2009) Maintaining network activity in submerged hippocampal slices: importance of oxygen supply. Eur J Neurosci 29: 319–327.
26. Maier N, Morris G, Johenning FW, Schmitz D (2009) An approach for reliably investigating hippocampal sharp wave-ripples in vitro. PLoS One 4: e6925.
27. Reichinnek S, von Kameke A, Hagenston AM, Freitag E, Roth FC, et al. (2012) Reliable optical detection of coherent neuronal activity in fast oscillating networks in vitro. Neuroimage 60: 139–152.
28. O'Neill J, Senior T, Csicsvari J (2006) Place-selective firing of CA1 pyramidal cells during sharp wave/ripple network patterns in exploratory behavior. Neuron 49: 143–155.
29. Huang YY, Kandel ER (1995) D1/D5 receptor agonists induce a protein synthesis-dependent late potentiation in the CA1 region of the hippocampus. Proc Natl Acad Sci U S A 92: 2446–2450.
30. Papatheodoropoulos C (2008) A possible role of ectopic action potentials in the in vitro hippocampal sharp wave-ripple complexes. Neuroscience 157: 495–501.
31. Bahner F, Weiss EK, Birke G, Maier N, Schmitz D, et al. (2011) Cellular correlate of assembly formation in oscillating hippocampal networks in vitro. Proc Natl Acad Sci U S A 108: E607–616.
32. Ellender TJ, Nissen W, Colgin LL, Mann EO, Paulsen O (2010) Priming of hippocampal population bursts by individual perisomatic-targeting interneurons. J Neurosci 30: 5979–5991.
33. Aivar P, Valero M, Bellistri E, Menendez de la Prida L (2014) Extracellular calcium controls the expression of two different forms of ripple-like hippocampal oscillations. J Neurosci 34: 2989–3004.
34. Csicsvari J, Hirase H, Mamiya A, Buzsaki G (2000) Ensemble patterns of hippocampal CA3-CA1 neurons during sharp wave-associated population events. Neuron 28: 585–594.
35. Klausberger T, Somogyi P (2008) Neuronal diversity and temporal dynamics: the unity of hippocampal circuit operations. Science 321: 53–57.
36. Takahashi N, Oba S, Yukinawa N, Ujita S, Mizunuma M, et al. (2011) High-speed multineuron calcium imaging using Nipkow-type confocal microscopy. Curr Protoc Neurosci 2: 14.
37. Sasaki T, Matsuki N, Ikegaya Y (2007) Metastability of active CA3 networks. J Neurosci 27: 517–528.
38. Sasaki T, Matsuki N, Ikegaya Y (2014) Interneuron firing precedes sequential activation of neuronal ensembles in hippocampal slices. Eur J Neurosci 39: 2027–2036.
39. Freund TF, Buzsaki G (1996) Interneurons of the hippocampus. Hippocampus 6: 347–470.
40. Mizunuma M, Norimoto H, Tao K, Egawa T, Hanaoka K, et al. (2014) Unbalanced excitability underlies offline reactivation of behaviorally activated neurons. Nat Neurosci 17: 503–505.
41. Frey BJ, Dueck D (2007) Clustering by passing messages between data points. Science 315: 972–976.
42. Takahashi N, Sasaki T, Matsumoto W, Matsuki N, Ikegaya Y (2010) Circuit topology for synchronizing neurons in spontaneously active networks. Proc Natl Acad Sci U S A 107: 10244–10249.
43. Ibarz JM, Foffani G, Cid E, Inostroza M, Menendez de la Prida L (2010) Emergent dynamics of fast ripples in the epileptic hippocampus. J Neurosci 30: 16249–16261.
44. Schomburg EW, Anastassiou CA, Buzsaki G, Koch C (2012) The spiking component of oscillatory extracellular potentials in the rat hippocampus. J Neurosci 32: 11798–11811.
45. Weiss T, Veh RW, Heinemann U (2003) Dopamine depresses cholinergic oscillatory network activity in rat hippocampus. Eur J Neurosci 18: 2573–2580.
46. Hasselmo ME (1999) Neuromodulation: acetylcholine and memory consolidation. Trends Cogn Sci 3: 351–359.
47. Zylla MM, Zhang X, Reichinnek S, Draguhn A, Both M (2013) Cholinergic plasticity of oscillating neuronal assemblies in mouse hippocampal slices. PLoS One 8: e80718.
48. Reichinnek S, Kunsting T, Draguhn A, Both M (2010) Field potential signature of distinct multicellular activity patterns in the mouse hippocampus. J Neurosci 30: 15441–15449.
49. Vogels TP, Sprekeler H, Zenke F, Clopath C, Gerstner W (2011) Inhibitory plasticity balances excitation and inhibition in sensory pathways and memory networks. Science 334: 1569–1573.
50. Maier N, Tejero-Cantero A, Dorrn AL, Winterer J, Beed PS, et al. (2011) Coherent phasic excitation during hippocampal ripples. Neuron 72: 137–152.
51. Carr MF, Jadhav SP, Frank LM (2011) Hippocampal replay in the awake state: a potential substrate for memory consolidation and retrieval. Nat Neurosci 14: 147–153.
52. Dragoi G, Tonegawa S (2011) Preplay of future place cell sequences by hippocampal cellular assemblies. Nature 469: 397–401.
53. Singer AC, Carr MF, Karlsson MP, Frank LM (2013) Hippocampal SWR activity predicts correct decisions during the initial learning of an alternation task. Neuron 77: 1163–1173.
54. Suh J, Foster DJ, Davoudi H, Wilson MA, Tonegawa S (2013) Impaired hippocampal ripple-associated replay in a mouse model of schizophrenia. Neuron 80: 484–493.
55. Witten IB, Steinberg EE, Lee SY, Davidson TJ, Zalocusky KA, et al. (2011) Recombinase-driver rat lines: tools, techniques, and optogenetic application to dopamine-mediated reinforcement. Neuron 72: 721–733.
56. Lee TH, Gee KR, Ellinwood EH, Seidler FJ (1996) Combining 'caged-dopamine' photolysis with fast-scan cyclic voltammetry to assess dopamine clearance and release autoinhibition in vitro. J Neurosci Methods 67: 221–231.
57. Breier A, Su TP, Saunders R, Carson RE, Kolachana BS, et al. (1997) Schizophrenia is associated with elevated amphetamine-induced synaptic dopamine concentrations: evidence from a novel positron emission tomography method. Proc Natl Acad Sci U S A 94: 2569–2574.
58. Sun Y, Norimoto H, Pu XP, Matsuki N, Ikegaya Y (2012) Cannabinoid receptor activation disrupts the internal structure of hippocampal sharp wave-ripple complexes. J Pharmacol Sci 118: 288–294.
59. Ikegaya Y, Aaron G, Cossart R, Aronov D, Lampl I, et al. (2004) Synfire chains and cortical songs: temporal modules of cortical activity. Science 304: 559–564.

Brief Communications

Synaptic Plasticity Associated with a Memory Engram in the Basolateral Amygdala

Ayako Nonaka,[1]* Takeshi Toyoda,[1]* Yuki Miura,[1] Natsuko Hitora-Imamura,[1] Masamitsu Naka,[1] Megumi Eguchi,[2] Shun Yamaguchi,[2,3] Yuji Ikegaya,[1,4] Norio Matsuki,[1] and Hiroshi Nomura[1]

[1]Laboratory of Chemical Pharmacology, Graduate School of Pharmaceutical Sciences, The University of Tokyo, Tokyo 113-0033, Japan, [2]Division of Morphological Neuroscience, Gifu University Graduate School of Medicine, Gifu 501-1194, Japan, [3]PRESTO, Japan Science and Technology Agency (JST), Saitama 332-0012, Japan, and [4]Center for Information and Neural Networks, Suita City, Osaka 565-0871, Japan

Synaptic plasticity is a cellular mechanism putatively underlying learning and memory. However, it is unclear whether learning induces synaptic modification globally or only in a subset of neurons in associated brain regions. In this study, we genetically identified neurons activated during contextual fear learning and separately recorded synaptic efficacy from recruited and nonrecruited neurons in the mouse basolateral amygdala (BLA). We found that the fear learning induces presynaptic potentiation, which was reflected by an increase in the miniature EPSC frequency and by a decrease in the paired-pulse ratio. Changes occurred only in the cortical synapses targeting the BLA neurons that were recruited into the fear memory trace. Furthermore, we found that fear learning reorganizes the neuronal ensemble responsive to the conditioning context in conjunction with the synaptic plasticity. In particular, the neuronal activity during learning was associated with the neuronal recruitment into the context-responsive ensemble. These findings suggest that synaptic plasticity in a subset of BLA neurons contributes to fear memory expression through ensemble reorganization.

Introduction

One cellular mechanism underlying fear conditioning is likely to be synaptic plasticity in the amygdala. Fear conditioning potentiates synaptic strength in the amygdala (McKernan and Shinnick-Gallagher, 1997; Tsvetkov et al., 2002) and is impaired when synaptic plasticity in the amygdala is inhibited (Fanselow and Kim, 1994; Rumpel et al., 2005). However, it is unclear whether fear learning induces synaptic modification in the amygdala globally or only in a subset of neurons. Because studies using activity-dependent gene expression showed that a subset of amygdala neurons are involved in fear conditioning (Han et al., 2007, 2009; Reijmers et al., 2007), we hypothesized that fear learning induces synaptic modification only in neurons that are recruited into the memory trace. Furthermore, if this is the case, synaptic modification in a subset of neurons would likely lead to a reorganization of amygdala neuronal ensemble activity.

Received Sept. 25, 2013; revised May 20, 2014; accepted June 5, 2014.

Author contributions: Y.I., N.M., and H.N. designed research; A.N., T.T., Y.M., N.H.-I., M.N., and H.N. performed research; M.E. and S.Y. contributed unpublished reagents/analytic tools; A.N., T.T., Y.M., and H.N. analyzed data; A.N. and H.N. wrote the paper.

This work was supported by a Grant-in-Aid for Young Scientists (B) (25830002 to H.N.); Grant-in-Aid for Scientific Research on Innovative Areas, "Mesoscopic Neurocircuitry" (23115101 to H.N.); "The Science of Mental Time" (26119507 to H.N. and 25119004 to Y.I.); and "Memory Dynamism" (26115509 to H.N.). We thank Dr. Hiroyuki Hioki (Kyoto University) for technical advice in *in situ* hybridization and immunohistochemistry, Dr. Paul F Worley (Johns Hopkins University) for the *Arc* and *Homer 1a* cDNA used in this study, and the University of Tokyo/Leica microsystems imaging center for their assistance in obtaining the imaging data.

*A.N. and T.T. contributed equally to this work.

The authors declare no competing financial interests.

Correspondence should be addressed to Hiroshi Nomura, PhD, Laboratory of Chemical Pharmacology, Graduate School of Pharmaceutical Sciences, The University of Tokyo 7-3-1 Hongo, Bunkyo-ku, Tokyo 113-0033, Japan. E-mail: nomura@mol.f.u-tokyo.ac.jp.

DOI:10.1523/JNEUROSCI.4233-13.2014

 0270-6474/14/349305-05$15.00/0

Here, we tested these ideas by combining whole-cell recordings with imaging of neuronal activity histories. We examined synaptic plasticity and ensemble reorganization associated with contextual fear conditioning. Further, we focused our analysis on the basolateral amygdala (BLA) because of its importance in contextual fear conditioning (Maren, 2001).

Materials and Methods

Animals. All experiments were approved by the animal experiment ethics committee at the University of Tokyo (approval number 24-8, 24-10), and were in accordance with the University of Tokyo guidelines for the care and use of laboratory animals. For catFISH, we used male C57BL/6J mice (8–15 weeks old; SLC) on a 12 h light/dark cycle with lights on from 7:00 A.M. to 7:00 P.M., with access to food and water *ad libitum*. For electrophysiological experiments, we used male or female *Arc-dVenus* transgenic mice (3–5 weeks old; Eguchi and Yamaguchi, 2009).

Behavioral procedures. In the electrophysiological experiments with fear memory retrieval (Fig. 1), we examined synaptic efficacy in the neurons that were activated during memory retrieval. On day 1, mice in the fear conditioning (FC) group were conditioned in a conditioning chamber with three footshocks (1 mA, 2 s, 150 s intervals). Mice in the immediate shock (IS) group received a footshock (1 mA, 6 s) immediately after they were placed in the chamber. On day 2, both groups were re-exposed to the chamber for 5 min and killed 5 h later, when dVenus fluorescence reaches a plateau (Eguchi and Yamaguchi, 2009). In the electrophysiological experiments without fear memory retrieval (Fig. 2), we examined synaptic efficacy in the neurons that were activated during fear conditioning. Mice were conditioned in the conditioning chamber with three footshocks and killed 5 h later.

In the catFISH experiments that examined fear conditioning-induced ensemble reorganization, the behavioral test comprised three sessions. In session 1, mice in the FC group were placed in the conditioning chamber for 5 min. The mice were returned to their home cage and 36 min later, in session 2, they were conditioned with three footshocks (1 mA, 2 s, 150 s

intervals) in the chamber. They were returned to their home cage again, and 20 min later (session 3) they were re-exposed to the chamber for 5 min to induce recall of the fear memory. The IS group, a control for associative learning, was given footshocks 0, 10, and 20 s after being placed in the chamber in session 2, instead of the fear conditioning protocol. In the catFISH experiments that examined the time course of the cytoplasmic *Homer 1a* signals, mice were exposed to the conditioning chamber for 5 min without shock. They were killed immediately, 25 min or 70 min after the context exposure.

All sessions were video recorded to enable the automatic scoring of freezing behavior according to the previously described method (Nomura and Matsuki, 2008).

Electrophysiology. Mice were deeply anesthetized with diethyl ether and decapitated 5 h after re-exposure to the conditioning context. Brains were removed quickly, and coronal slices (300 μm thick) containing the BLA were prepared with a vibratome (VT 1200S; Leica) in ice-cold, oxygenated (95% O_2/5% CO_2) modified artificial CSF (mACSF) containing 222.1 mM sucrose, 27 mM $NaHCO_3$, 1.4 mM NaH_2PO_4, 2.5 mM KCl, 0.5 mM ascorbic acid, 1 mM $CaCl_2$, and 7 mM $MgSO_4$.

Picrotoxin (100 μM) was added to ACSF (127 mM NaCl, 1.6 mM KCl, 1.24 mM KH_2PO_4, 1.3 mM $MgSO_4$, 2.4 mM $CaCl_2$, 26 mM $NaHCO_3$, and 10 mM glucose). Whole-cell patch-clamp recordings were performed with glass microelectrodes (3–8 MΩ) filled with internal solution (135 mM K-gluconate, 4 mM KCl, 10 mM phosphocreatine-Na_2, 10 mM HEPES, 4 mM MgATP, and 0.3 mM Na_2GTP, pH 7.2–7.3, 280–295 mOsm). Because the BLA receives projections from diverse cortices and thalamus including the entorhinal and perirhinal cortices and mediodorsal thalamic nucleus, which are involved in contextual fear conditioning (Maren and Fanselow, 1997; Sacchetti et al., 1999; Li et al., 2004), we examined the effect of contextual fear conditioning on the cortico-BLA and thalamo-BLA synapses. Electrical stimulation was applied to the internal capsule to evoke EPSCs in BLA neurons from thalamic afferents, or to the external capsule to evoke EPSCs from cortical afferents, using bipolar tungsten electrodes (0.1–1 MΩ). Paired stimuli were given with an interstimulus interval of 50 ms, and the ratio between the amplitude of the second and first EPSCs was calculated. Miniature EPSCs (mEPSCs) were recorded at a holding potential of −70 mV in the presence of tetrodotoxin (1 μM). mEPSCs were detected using an in-house MATLAB program and were defined as inward currents with amplitudes >7 pA unless stated (Miura et al., 2012). Data were sampled at 20 kHz and filtered at 2 kHz using an Axopatch 200B, 700B amplifier (Molecular Devices), DIGIDATA1320A, 1440A (Molecular Devices), and pClamp 10.2 (Molecular Devices). All data were acquired, stored, and analyzed using Clampex 10, Clampfit, and MATLAB.

Fluorescence in situ hybridization. Mice were killed immediately after session 3, and their brains were removed and frozen quickly. *In situ* hybridization was performed according to previously published protocols (Nomura et al., 2012). The coronal brain sections (20 μm) were hybridized with the riboprobes (DIG-*Homer 1a* antisense riboprobe, 2 μg/ml; Fluorescein-*Arc* antisense riboprobe, 1 μg/ml). The signals were detected with an anti-Fluorescein HRP-conjugated antibody (1:200; PerkinElmer); a TSA Plus DNP System (1:10; PerkinElmer); an anti-DIG peroxidase-conjugated antibody (1:500; Roche); Tyramide-biotin (1:5000), an Alexa488-conjugated anti-DNP antibody (Invitrogen); and Alexa594-conjugated streptavidin (Invitrogen). The nuclei were counterstained with Hoechst.

Z-stacks of 1-μm-thick optical sections were acquired with LSM-510 (Zeiss) and CV1000 (Yokogawa Denki) confocal microscopes using 40× objective lenses. Only cells that were presumptive neurons with whole, large nuclei stained diffusely with the Hoechst dye were included in the analysis. The designation "intranuclear positive" was assigned to neurons that exhibited one or two of the characteristic intense intranuclear areas of fluorescence. The designation "cytoplasmic positive" was assigned to neurons that contained perinuclear/cytoplasmic labeling over multiple optical sections.

Immunohistochemistry. For dVenus detection, mice were transcardially perfused with 4% PFA in PBS 5 h after re-exposure to the conditioning context. The sections were incubated with rabbit anti-GFP antibody (1:1000; Invitrogen), Alexa488 anti-rabbit IgG (1:500; Invitrogen), and NeuroTrace Blue (1:50; Invitrogen).

Data analysis. All values are given as the mean ± SEM. Two-way factorial ANOVA, repeated-measure ANOVA, Student's *t* test, the Tukey–Kramer test, and the paired *t* test were used for appropriate comparisons.

An overlap score between neuronal populations that were active during both sessions 1 and 3 was obtained as follows: S_1 = percentage of total cytoplasmic *Homer 1a*+ neurons, S_3 = percentage of total nuclear *Arc*+ neurons, S_{13} = percentage of neurons in which both cytoplasmic *Homer 1a* and nuclear *Arc* were observed, chance level (C_{13}) = $S_1 \times S_3/100$, overlap score between sessions 1 and 3 = $(S_{13} - C_{13})/(S_3 - C_{13}) \times 100$. The recruiting score was calculated as the percentage of neurons that changed their activity from inactive in session 1 to active in session 3.

Results

Contextual fear conditioning induces presynaptic potentiation in BLA neurons recruited into a fear memory trace

To identify the neurons that were recruited into a memory trace, we used *Arc-dVenus* transgenic mice. These mice express a destabilized version of the fluorescent protein Venus under the control of the *Arc* promoter (Eguchi and Yamaguchi, 2009). The *Arc-dVenus* mice allowed us to identify the neurons that were recruited into the memory trace by dVenus fluorescence produced by *Arc* activation during fear memory expression. The mice received contextual fear conditioning, and 24 h later they were re-exposed to the conditioning context (Fig. 1*A*). They showed robust freezing during the re-exposure to the context (Fig. 1*B*), suggesting that they recalled the contextual fear memory. They were killed 5 h after the context re-exposure for the subsequent electrophysiological studies. An IS group, which received a footshock immediately after they were placed in the chamber, was prepared as a control for associative fear learning (Fig. 1*B*). The percentage of dVenus+ BLA neurons in FC mice was higher than that of home cage (HC) controls (Fig. 1*C*,*D*).

Brain slices were prepared for whole-cell recordings from BLA neurons. We measured mEPSCs from dVenus+ (V+) and dVenus− (V−) neurons of the mice in the FC and IS groups. The mEPSC frequency of the dVenus+ neurons in the FC group was higher than that of the dVenus− neurons in the FC group and the dVenus+ neurons in the IS group (Fig. 1*E*,*F*). There was no significant group × dVenus interaction for mEPSC amplitude (Fig. 1*G*).

To probe the synaptic efficacy of dVenus+ neurons in the FC group, we measured the evoked EPSCs and paired-pulse ratio (PPR). The EPSC amplitude of the dVenus+ neurons in the FC group was higher than that of the dVenus− neurons in the FC group in the cortical, but not the thalamic, pathway (Fig. 1*H*,*I*). PPR in the dVenus+ neurons of the FC group was lower than that in dVenus− neurons of the FC group in the cortical, but not the thalamic, pathway (Fig. 1*J*,*K*). These results indicate that the synaptic efficacy of cortico-amygdala synapses is presynaptically enhanced in the FC group, and that this enhancement is restricted to neurons that were recruited into the memory trace (i.e., dVenus+ neurons).

We tested whether fear memory retrieval is required for the high mEPSC frequency in the recruited neurons. *Arc-dVenus* mice were killed 5 h after they received fear conditioning without re-exposure to the conditioning context (Fig. 2*A*). BLA dVenus+ neurons showed higher mEPSC frequency and amplitude than dVenus− neurons (Fig. 2*B*–*D*). These results suggest that the high mEPSC frequency in the recruited neurons is attributable to fear conditioning.

In all the analyses described above, we detected mEPSCs with a 7 pA threshold. This analysis strictly removed noise (false positive EPSCs) but could miss small mEPSCs. To avoid missing

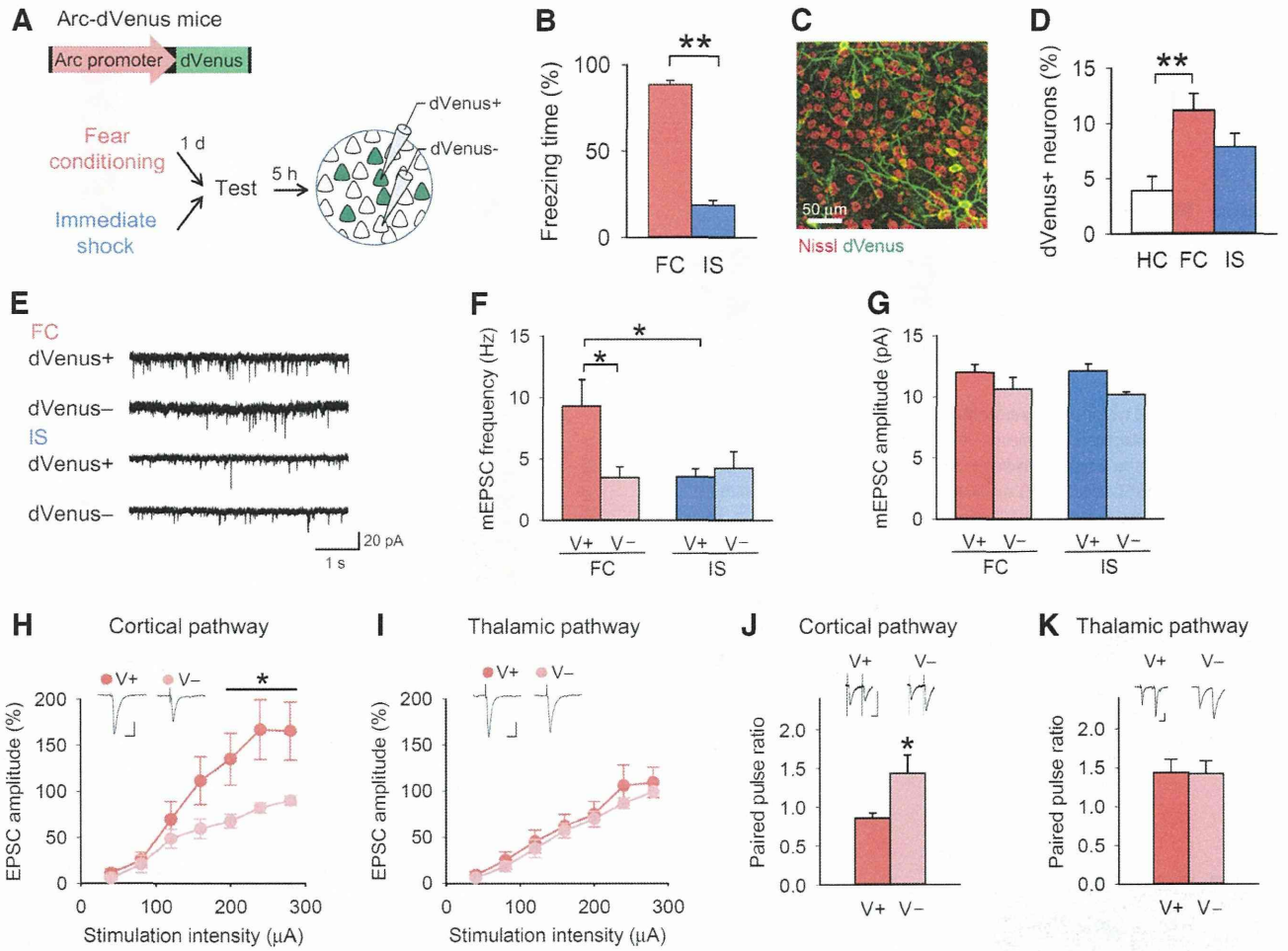

Figure 1. Contextual fear conditioning induces presynaptic potentiation in BLA neurons recruited into a fear memory trace. ***A***, Experimental procedure. ***B***, The FC group showed longer freezing time during the test than the IS group. ***C***, A representative fluorescence image of BLA neurons with dVenus. ***D***, Re-exposure to the conditioning context increased the proportion of dVenus+ neurons in the BLA (one-way ANOVA, $F_{(2,18)} = 6.7$, $p = 0.0068$; Tukey's test, home cage (HC) vs FC, $p = 0.0050$). ***E***, ***F***, dVenus+ (V+) neurons of the FC group had a higher mEPSC frequency than dVenus− (V−) neurons of the FC group and dVenus+ neurons of the IS group ($n = 10$ dVenus+ and 10 dVenus− neurons per behavioral group from 14 mice in the FC group and 12 mice in the IS group; two-way ANOVA, $F_{(1,36)} = 4.9$, $p = 0.033$; dVenus+ (FC) vs dVenus− (FC), $p = 0.042$; dVenus+ (FC) vs dVenus+ (IS), $p = 0.024$). ***G***, There was no significant group × dVenus interaction of mEPSC amplitude ($F_{(1,36)} = 0.33$, $p = 0.57$). ***H***, ***I***, The EPSC amplitude of the dVenus+ neurons in the FC group was higher than that of the dVenus− neurons in the FC group in the cortical but not thalamic pathway ($n = 7$–10 neurons from 5 mice; cortical pathway, repeated-measures ANOVA, $F_{(6,108)} = 4.5$, $p = 4.1 \times 10^{-4}$). Calibration: 20 ms, 100 pA. ***J***, ***K***, The PPR in dVenus+ neurons in the FC group was lower than that of dVenus− neurons in the FC group in the cortical but not thalamic pathway ($n = 7$–11 neurons from 7 mice; cortical pathway, Student's t test, $t_{(11)} = 2.3$, $p = 0.041$). Calibration: 20 ms, 50 pA. $^{**}p < 0.01$, $^{*}p < 0.05$.

small mEPSCs, we also performed an additional analysis detecting mEPSCs with a 5 pA threshold. Similarly with the 7 pA threshold analyses, we found that BLA dVenus+ neurons showed a higher mEPSC frequency (dVenus+: 12.1 ± 2.8 Hz; dVenus−: 6.9 ± 2.1 Hz; paired t test, $t_{(5)} = 4.7$, $p = 0.0051$) and amplitude (dVenus+: 10.0 ± 0.19 pA; dVenus−: 8.3 ± 0.14; $t_{(5)} = 9.9$, $p = 0.0002$) than dVenus− neurons.

Fear conditioning reorganizes a context-responsive BLA neuronal ensemble based on the activity of individual BLA neurons during fear conditioning

Because synaptic potentiation in a subset of neurons is likely to lead to a reorganization of neuronal ensembles, we tested whether a BLA neuronal ensemble responsive to context is altered by fear conditioning. Mice in the FC group were subjected to context exposure in session 1 (S1), contextual fear conditioning in session 2 (S2), and context re-exposure in session 3 (S3) with 36 and 20 min intervals (Fig. 3*A*). They spent a much greater time freezing in session 3 versus session 1 (Fig. 3*B*). The IS group demonstrated significantly less freezing in session 3 than the FC group.

To identify neurons that were active during each session, we used temporal activity mapping with cellular resolution by observing *Arc* and *Homer 1a* RNA (i.e., catFISH; Guzowski et al., 1999; Marrone et al., 2008). Transcribed *Arc* RNA first appears in neuronal nuclei, after which processed *Arc* mRNA accumulates in the cytoplasm. *Homer 1a* RNA is transcribed later than *Arc* RNA. Previously, we reported that nuclear *Arc* is observed immediately after neuronal activity and that cytoplasmic *Arc* and nuclear *Homer 1a* are observed 25–30 min after neuronal activity in the amygdala (Hashikawa et al., 2011; Nomura et al., 2012). Because the characteristics of the cytoplasmic *Homer 1a* signal have been described for hippocampal neurons (Marrone et al., 2008) but not amygdala neurons, we first examined the time course of the cytoplasmic *Homer 1a* signal after neuronal activity. We found that in the basolateral amygdala, as well as the hippocampal CA1, more cytoplasmic *Homer 1a*+ neurons were observed when mice were killed 70 min after context exposure compared